Analysis of the Cob(II)alamin−5′-Deoxy-3′,4′-anhydroadenosyl Radical Triplet Spin System in the Active Site of Diol Dehydrase†

Steven O. Mansoorabadi,‡ Olafur Th. Magnusson,§ Russell R. Poyner, Perry A. Frey, and George H. Reed*

Department of Biochemistry, University of Wisconsin, Madison, Wisconsin 53726-4087

Received August 4, 2006; Revised Manuscript Received October 3, 2006

ABSTRACT: A triplet spin system ($S = 1$) is detected by low-temperature electron paramagnetic resonance (EPR) spectroscopy in samples of diol dehydrase and the functional adenosylcobalamin (AdoCbl) analogue 5′-deoxy-3′,4′-anhydroadenosylcobalamin (*an*AdoCbl). Different spectra are observed in the presence and absence of the substrate (*R*,*S*)-1,2-propanediol. In both cases, the spectra include a prominent half-field transition ($\Delta M_S = 2$) that is a hallmark of strongly coupled triplet spin systems. The appearance of ^{59}Co hyperfine splitting in the EPR signals and the positions (*g* values) of the signals in the spectra show that half of the triplet spin is contributed by the low-spin Co^{2+} of cob(II)alamin. Line width effects from isotopic labeling (^{13}C and ^{2}H) in the 5′-deoxy-3′,4′-anhydroribosyl ring demonstrate that the other half of the spin triplet is from an allylic 5′-deoxy-3′,4′-anhydroadenosyl (anhydroadenosyl) radical. The zero-field splitting (ZFS) tensors describing the magnetic dipole−dipole interactions of the component spins of the triplets have rhombic symmetry because of electron spin delocalization within the organic radical component and the proximity of the radical to the low-spin Co^{2+}. The dipole−dipole interaction was modeled as a summation of point−dipole interactions involving the spin-bearing orbitals of the anhydroadenosyl radical and cob(II)alamin. Geometries which are consistent with the ZFS tensors in the presence and absence of the substrate position the 5′-carbon of the anhydroadenosyl radical 3.5 and 4.1 Å from Co^{2+}, respectively. Homolytic cleavage of the cobalt−carbon bond of the analogue in the absence of the substrate indicates that, in diol dehydrase, binding of the coenzyme to the protein weakens the bond prior to binding of the substrate.

A common characteristic of adenosylcobalamin-dependent enzymes is the generation and utilization of enzyme-bound organic radicals (*1*−*3*). The Co−C5′ bond of AdoCbl[1] is relatively weak, having a bond dissociation energy of ∼30 kcal/mol (*4*). A prevalent mechanism for AdoCbl-dependent enzymes begins with the homolytic cleavage of the Co−C5′ bond to give cob(II)alamin and the 5′-deoxyadenosyl radical (*1*). The 5′-deoxyadenosyl radical being an unstabilized, primary alkyl radical is expected to have a short lifetime, a low concentration, and a high reactivity toward H atom abstraction. Thus far, these properties of the 5′-deoxyadenosyl radical have precluded direct observation of the radical by EPR spectroscopy. Cleavage of the Co−C5′ bond is kinetically coupled to abstraction of a H atom from a substrate molecule in the reactions of methylmalonyl-CoA mutase (*5*), glutamate mutase (*6*), ethanolamine ammonia lyase (*7*), and diol dehydrase (*8*). These kinetic experiments have highlighted the transient nature of the 5′-deoxyadenosyl radical species. In the case of the AdoCbl-dependent class II ribonucleoside triphosphate reductase, the 5′-deoxyadenosyl radical abstracts a H atom from the thiol of Cys408 of the protein (*9*). An allosteric effector-dependent epimerization of chiral [5′-$^{2}H_1$]AdoCbl by the C408A and C408S mutant forms of the enzyme requires the transient existence of the 5′-deoxyadenosyl radical (*10*).

DDH (diol dehydrase, EC 4.2.1.28) uses two- and three-carbon vicinal diols as substrates and catalyzes their transformation into aldehydes (*8*, *11*). The minimal mechanism for DDH with 1,2-propanediol as the substrate is depicted in Scheme 1. Reversible cleavage of the Co−C5′ bond of AdoCbl generates 5′-deoxyadenosyl radical **a**, which abstracts a hydrogen atom from C1 of 1,2-propanediol to produce 5′-deoxyadenosine **b** and substrate radical **c**. The substrate radical undergoes isomerization to product-related radical **d** by an unknown mechanism. Hypothetical mechanisms for the radical rearrangement include the formation of a radical cation (*12*) or a radical anion intermediate (*13*). Concerted mechanisms having transition state stabilization by partial proton transfer or deprotonation of the spectator OH group have also been discussed (*14*, *15*). Crystal structures of DDH reveal that the vicinyl OH groups of 1,2-

† This research was supported by NIH Grants GM35752 (G.H.R.) and DK28607 (P.A.F.). S.O.M. was supported in part by NIH Predoctoral Training Grant T32 GM08293 in molecular biophysics.

* To whom correspondence should be addressed: University of Wisconsin, 1710 University Ave., Madison, WI 53726-4087. Telephone: (608) 262-0509. Fax: (608) 265-2904. E-mail: reed@biochem.wisc.edu.

‡ Present address: Department of Medicinal Chemistry, University of Texas College of Pharmacy, Austin, TX 78712.

§ Present address: deCode Genetics/Drug Discovery, Sturlugata 8, IS-101 Reykjavik, Iceland.

[1] Abbreviations: AdoCbl, 5′-deoxyadenosylcobalamin; *an*AdoCbl, 5′-deoxy-3′,4′-anhydroadenosylcobalamin; *an*ATP, 3′,4′-anhydroadenosine triphosphate; anhydroadenosyl radical, 5′-deoxy-3′,4′-anhydroadenosyl radical; BDE, bond dissociation energy; DMB, dimethylbenzimidazole; DDH, diol dehydrase; EPR, electron paramagnetic resonance; ENDOR, electron nuclear double resonance; SAM, *S*-adenosyl-L-methionine; ZFS, zero-field splitting; rmsd, root-mean-square deviation.

10.1021/bi061586q CCC: $33.50 © 2006 American Chemical Society
Published on Web 11/09/2006

Scheme 1

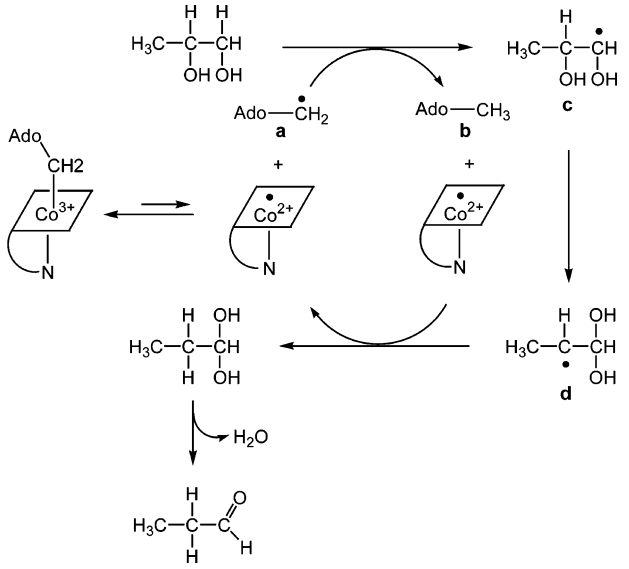

Scheme 2

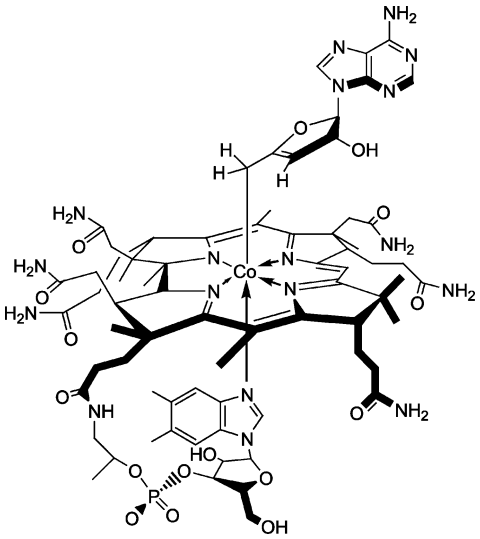

propanediol are coordinated to K^+, and K^+ may be involved in catalysis (*16*, *17*). Magnetic interactions between active site radicals and the nuclear spins of ^{39}K and $^{203,205}Tl$ have, however, escaped detection by EPR and ENDOR (*18*). Moreover, site-directed mutagenesis has revealed essential roles of Gluα170 and Aspα335 (*19*) in putative H-bonding contacts with the vicinal OH groups of the substrate. Transfer of hydrogen from 5′-deoxyadenosine **b** to radical **d** regenerates the 5′-deoxyadenosyl radical, which recombines with cob(II)alamin. The enzyme catalyzes the dehydration of the *gem*-diol to complete the reaction (*20*). Reactions of the DDH−AdoCbl complex with substrates or inhibitors elicit EPR signals corresponding to organic radicals spin coupled to the low-spin Co^{2+} of cob(II)alamin (*18*, *21*−*26*).

*an*AdoCbl, shown in Scheme 2, is an analogue of AdoCbl. *an*AdoCbl has a Co−C5′ bond dissociation energy which is ∼6 kcal/mol weaker than that of the corresponding bond in AdoCbl (*27*). The weakened Co−C5′ bond in *an*AdoCbl is attributed to allylic stabilization in the anhydroadenosyl radical relative to the 5′-deoxyadenosyl radical. Structures of the two radicals are compared in Scheme 3. *an*AdoCbl is a functional coenzyme for DDH, displaying a turnover rate

Scheme 3

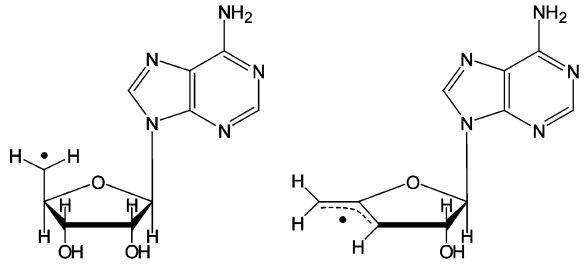

that is 0.02% of that with AdoCbl as the coenzyme (*28*). Binding of *an*AdoCbl to DDH induces cleavage of the Co−C5′ bond. Co−C5′ bond cleavage is observed spectrophotometrically as the formation of cob(II)alamin either in the presence or in the absence of the substrate (*28*). However, the enzyme undergoes slow inactivation as observed by the formation of cob(III)alamin, irrespective of the presence of the substrate. Inactivation is a consequence of the transfer of an electron from cob(II)alamin to the anhydroadenosyl radical and subsequent quenching of the allylic anion by a solvent-derived proton (*28*).

Cleavage of the Co−C5′ bond of *an*AdoCbl generates the anhydroadenosyl radical and cob(II)alamin in the active site of DDH. This paper presents EPR evidence of the presence of strongly coupled spin triplets involving the anhydroadenosyl radical and the low-spin Co^{2+} of cob(II)alamin in complexes of DDH with the cofactor analogue in the presence and absence of substrate. Analysis of the spin triplet EPR spectra by simulation and interpretation of the ZFS in terms of molecular geometries are presented.

EXPERIMENTAL PROCEDURES

Materials. Sodium cholate and AdoCbl were from Sigma. (*R*,*S*)-1,2-Propanediol was from Aldrich. (*R*,*S*)-1,2-[$^2H_6$]-Propanediol (99.5% ^2H) was from CDN Isotopes. All other solvents, buffers, and chemicals were obtained from either Fisher or Aldrich and used as supplied. *an*AdoCbl and [$^{13}C_5$-*ribosyl*]*an*AdoCbl were synthesized as described previously (*27*). The ^{13}C-labeled compound was prepared from the [$^{13}C_5$-*ribosyl*]*an*ATP precursor, the synthesis of which is described elsewhere (*29*). Recombinant DDH from *Salmonella typhimurium* was produced in *Escherichia coli* and purified and assayed as described previously (*28*, *30*).

Sample Preparation. Samples were prepared from solutions that were kept within a Coy anaerobic chamber. The samples contained 0.2 mM DDH in 10 mM potassium phosphate (pH 8), 0.5% sodium cholate buffer in a final volume of 0.25 mL, with either *an*AdoCbl (0.32 mM) or [$^{13}C_5$-*ribosyl*]*an*AdoCbl (0.3 mM) as the coenzyme. Samples prepared with the substrate contained either 0.12 M (*R*,*S*)-1,2-propanediol or 0.12 M (*R*,*S*)-1,2-[$^2H_6$]propanediol. Substrate-free samples were preincubated for 20 min with 1 μM AdoCbl before the coenzyme was added. This pretreatment with substoichiometric quantities of the normal cofactor ensured that residual traces of substrate, used to stabilize the enzyme during isolation and storage, would be converted to the product aldehyde. Samples were incubated at 25 °C for 1−10 min and transferred to EPR tubes, and the samples were frozen by immersing the tubes in cold isopentane (−135 °C).

EPR Spectroscopy. EPR spectra were recorded at cryogenic temperatures with a Varian spectrometer equipped with an E102 X-band microwave bridge, an Oxford Instruments ESR-900 continuous-flow helium cryostat, and an Oxford 3120 temperature controller. A Varian NMR gaussmeter, a Hewlett-Packard 5255A frequency converter, and a 5245L electronic counter were used to measure the magnetic field strength and microwave frequency. The spectrometer was interfaced with a computer for data acquisition. Spin concentrations were estimated by double integration and comparison with a CuEDTA standard in water and glycerol.

Spectral Simulations. Fourier filtering methods (*31*, *32*) were used to enhance the resolution in the EPR spectra. The spectra were analyzed using the following spin Hamiltonian:

$$H = \beta B g_1 S_1 + \beta B g_2 S_2 + S_1 D S_2 + J S_1 S_2 + H_{\mathrm{nuc}} \quad (1)$$

The first two terms in eq 1 represent the Zeeman interaction of the low-spin Co^{2+} of cob(II)alamin and the anhydroadenosyl radical with the external magnetic field, respectively; the third and fourth terms represent the magnetic dipole−dipole (ZFS)[2] and isotropic exchange interactions between cob(II)alamin and the anhydroadenosyl radical, respectively. H_{nuc} represents the nuclear hyperfine interactions:

$$H_{\mathrm{nuc}} = \sum_i I_i A_{i1} S_1 + \sum_j I_j A_{j2} S_2 \quad (2)$$

In general, Euler rotations (*33*) are needed to bring each of the tensors in eqs 1 and 2 into a common frame of reference, in this case the *g* axis system of Co^{2+}. However, the *g* tensors of organic radicals, such as the anhydroadenosyl radical, are very nearly isotropic, and thus, Euler angles are not required to align the two *g* tensors. Also, the nuclear hyperfine interactions of the anhydroadenosyl radical and of cob(II)alamin, other than with the ^{59}Co nucleus, are small relative to the ZFS and are safely neglected. The *g* tensor and ^{59}Co hyperfine tensor of cob(II)alamin are collinear. Therefore, the Euler angles aligning the ZFS tensor with the *g* tensor of cob(II)alamin (i.e., the angles relating the interspin vector to the *g* axis system of Co^{2+}) were the only angular variables in the fitting procedure. Energy levels and transition energies were obtained by diagonalization of the energy matrix. Field-swept powder EPR spectra were calculated as described previously (*34*). In this analysis, the ^{59}Co hyperfine interaction was treated to first-order, effectively reducing the energy matrix to a block diagonal form in the ^{59}Co nuclear quantum number, m_I. Initial estimates of the ZFS parameters were taken from the measured turning points in the experimental spectra, and the Co^{2+} *g* values and hyperfine parameters were obtained from previously reported values of cob(II)alamin bound to methylmalonyl-CoA mutase (*35*). These values were refined (changed slightly) by trial and error until reasonable fits were obtained.

The triplet state spectra in this study fall into the strongly exchange coupled regime, and in this regime, $|J|$ does not influence the positions of transitions in the spectra (*36*). Likewise, simulations were not sensitive to the sign of *J*. On the basis of the observation that the signals were much weaker at 77 K than at 4 K and the implied (large ZFS) short interspin distances, the exchange coupling is likely ferromagnetic. An "operational" value of $|J|$ of 40−50 cm^{-1} was used in the simulations. Given that the *g* tensor of the low-spin Co^{2+} is anisotropic and the interspin distances are short, there is a potential for anisotropic contributions from the exchange interaction (*36*, *37*). Given the modest Δg of low-spin Co^{2+}, complications from delocalized unpaired spins are likely more significant than anisotropic exchange in this system. The anisotropy has been treated exclusively as arising from the dipole−dipole interaction.

Analysis and Decomposition of the ZFS Tensor. Due to the delocalization of spin within the anhydroadenosyl radical, the size of the d_{z^2} orbital of Co^{2+}, and the proximity of these two paramagnetic centers, the commonly invoked point-dipole approximation (relating the ZFS to the distance between the spins) is not adequate for this system. To overcome the limitations of the point-dipole approximation, and to exploit the structural information implicit in the ZFS tensor, a multipoint model known as the point-charge model was used (*37*−*39*). In this model, fractional spins are assigned to individual atoms or orbital lobes. The resulting ensemble of fractional spins is treated by summing the multiple dipole−dipole interactions occurring between the two paramagnetic centers to generate the ZFS tensor (eq 3):

$$D_{ij} = \frac{\mu_o \beta^2}{4\pi} \sum_m \sum_n \rho_1(m)\rho_2(n) \frac{|\mathbf{r_2}(n) - \mathbf{r_1}(m)|^2 \delta_{ij} - 3[\mathbf{r_2}(n) - \mathbf{r_1}(m)]_i [\mathbf{r_2}(n) - \mathbf{r_1}(m)]_j}{|\mathbf{r_2}(n) - \mathbf{r_1}(m)|^5} \quad (3)$$

where δ_{ij} is the Kronecker delta, $\rho_1(m)$ and $\rho_2(n)$ are the spin densities of the *m*th and *n*th fractional spin of cob(II)alamin and the anhydroadenosyl radical, respectively, and $\mathbf{r_1}(m)$ and $\mathbf{r_2}(n)$ are the corresponding position vectors (*39*). The relative position of the two paramagnetic centers was obtained by minimizing (with the aid of a simulated annealing algorithm) the sum of the squared differences between the experimental ZFS tensor elements and those calculated with eq 3 (*40*, *41*). The search for reasonable local minima was guided by including in the objective function penalties to prevent unfavorable van der Waals contacts (*42*).

$$F = F_{\mathrm{D}}(1 + f_{\mathrm{vdw}}) \quad (4)$$

In eq 4, F_{D} has the form

$$F_{\mathrm{D}} = \sum_{i=1}^{2} \sum_{j=i}^{3} |D_{ij}^{\mathrm{exp}} - D_{ij}^{\mathrm{calc}}|^2$$

where the sum includes the six independent ZFS tensor elements (defined by *D*, *E*, and Euler angles ς, η, and ξ). f_{vdw} has the form

$$f_{\mathrm{vdw}} = \begin{cases} \sum_i \sum_j \left[\left(\frac{\sigma_{ij}}{r_{ij}} \right)^{12} - \left(\frac{\sigma_{ij}}{r_{ij}} \right)^{6} \right] & \text{for } \sigma_{ij} > r_{ij} \\ 0 & \text{for } \sigma_{ij} < r_{ij} \end{cases}$$

[2] The ZFS tensor used in the spin Hamiltonian has the form $D = g_1 D' g_2$, where D' is the ZFS tensor expressed in the principal axis system of g_1 divided by the square of the free electron *g* value. Using this formalism, contributions to the rhombicity of the ZFS from g_{xy} anisotropy are considered directly and separately from the contributions due to electron spin delocalization.

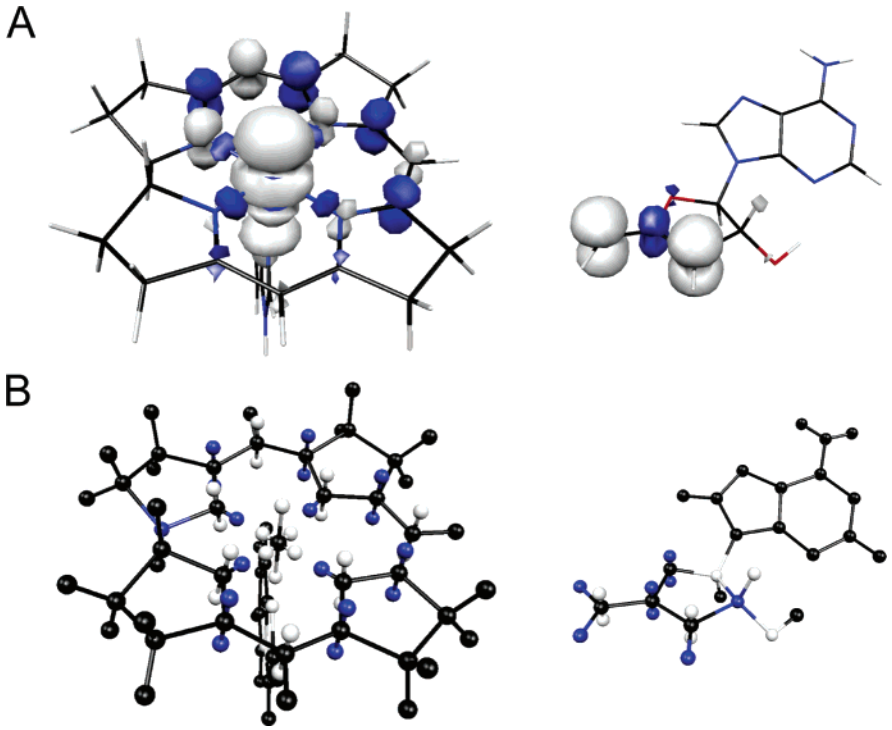

FIGURE 1: Comparison of isosurface spin densities obtained from *Gaussian 98* calculations (A) and the point-charge models used in the calculation of the ZFS tensor of the cob(II)alamin−anhydroadenosyl radical triplet system (B). Positive spin density is colored white and negative spin density blue. In the point-charge model, π-orbital lobes are positioned 0.7 Å above and below the molecular planes (*37*), σ-orbital lobes of the equatorial ring nitrogens are 0.5 Å from the nucleus along the Co−N bonds, and the d_{z^2} orbital lobes are positioned 1.1 Å above and below and 0.6 Å within the plane of the corrin ring.

where σ_{ij} is the van der Waals collision diameter between the *i*th atom of the anhydroadenosyl radical and the *j*th atom of cob(II)alamin and r_{ij} is the corresponding distance.

The spin densities used in eq 3 (see the Supporting Information) were obtained from single-point energy calculations on the anhydroadenosyl radical and a truncated cob(II)alamin structure using *Gaussian 98* (*43*). The geometries of the paramagnetic centers were optimized using Becke-style three-parameter density functional theory (DFT) with the Lee−Yang−Parr correlation functional (B3LYP) and Pople's polarized double-ζ 6-31G* basis set. Single-point calculations were performed on the optimized structures using the B3LYP hybrid functional in combination with the DFT-optimized valence triple-ζ basis set, TZVP. Isosurface plots of the spin densities of the anhydroadenosyl radical and the truncated cob(II)alamin are given in Figure 1A.

To better mimic the location of spin within the anhydroadenosyl radical, the spin density at each of the atoms in the π-system was divided in two and positioned equal distances above and below the plane of the anhydroribosyl ring (*38*). The atoms in the π-system of the corrin ring of cob(II)alamin were treated in an analogous fashion. The spin of the corrin ring nitrogen atoms was split into an additional point corresponding to the σ-orbital coordinating the low-spin Co^{2+}. The distribution of spin density within the d_{z^2} orbital of Co^{2+}, which can be expressed as a linear combination of $d_{(z^2-x^2)}$ and $d_{(z^2-y^2)}$ orbitals, was approximated by dividing the spin into six points, two equidistant above and below the plane and four equidistant within the plane of the corrin ring. The point-charge models of the anhydroadenosyl radical and cob(II)alamin that resulted in the best-fit ZFS tensors are illustrated in Figure 1B.

The starting coordinates for the analysis were obtained by placing the geometry-optimized cob(II)alamin fragment and the adenine ring of the anhydroadenosyl radical in the positions observed in the crystal structure of DDH complexed with adeninylpentylcobalamin (*44*). The position of the anhydroribosyl moiety was varied by rotation about the glycosidic bond, and small overall rotations and translations of the anhydroadenosyl radical were performed to find the best match of the experimentally observed and calculated ZFS tensors in the global minimization. The structure corresponding to the minimum in the analysis is not necessarily unique in its ability to reproduce the ZFS tensor. However, it represents the structure that best reproduces the ZFS tensor while minimizing changes in the geometry from that expected from the crystallographic data (*44*).

RESULTS AND DISCUSSION

EPR with anAdoCbl as the Coenzyme. EPR spectra of DDH with *an*AdoCbl as the coenzyme in the presence and absence of a saturating level of 1,2-propanediol are shown in Figures 2 and 3, respectively. These EPR spectra bear a resemblance to the strongly coupled triplet spectra detected in the AdoCbl-dependent enzymes ribonucleotide reductase (*45*), glutamate mutase (*46*), and methylmalonyl-CoA mutase (*47*−*49*), in that the signals are centered at *g* values midway between that of low-spin Co^{2+} and typical organic radicals and contain ^{59}Co hyperfine splittings that are contracted from that observed in magnetically isolated cob(II)alamin (*23*, *36*). However, the width of the EPR spectra in Figures 2 and 3 is much greater than that of any of the aforementioned triplet spectra, indicating that the distance separating the two paramagnetic centers comprising the spin triplets in this case is much shorter, resulting in a larger ZFS. The percentage

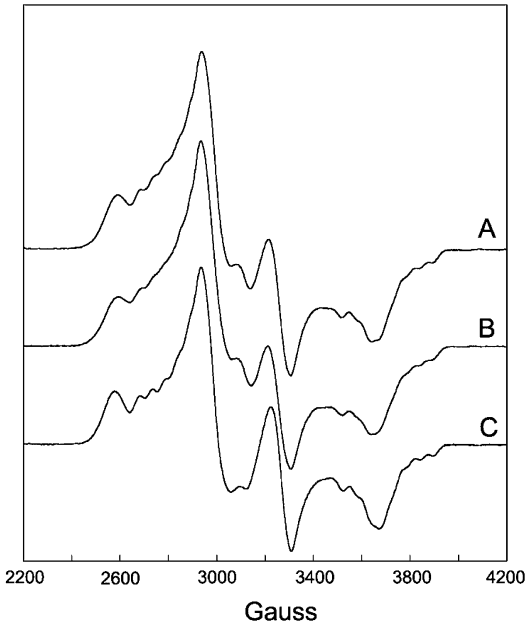

FIGURE 2: EPR spectra of DDH with *an*AdoCbl as the coenzyme in the presence of (*R*,*S*)-1,2-propanediol. The samples were frozen in cold isopentane 10 min after being mixed within an anaerobic chamber: (A) unlabeled coenzyme, (B) [$^{13}C_5$-*ribosyl*]*an*AdoCbl, and (C) *an*AdoCbl and (*R*,*S*)-1,2-[$^2H_6$]propanediol. Deuterium labeling at C5′ of the coenzyme occurs upon reaction with substrate. Experimental conditions: temperature, 4.5 K; modulation amplitude, 12 G; microwave power, 0.2 mW; spectrometer frequency, 9.233 GHz ($g = 2.0$ at 3299 G). All spectra are an average of four 8 min scans.

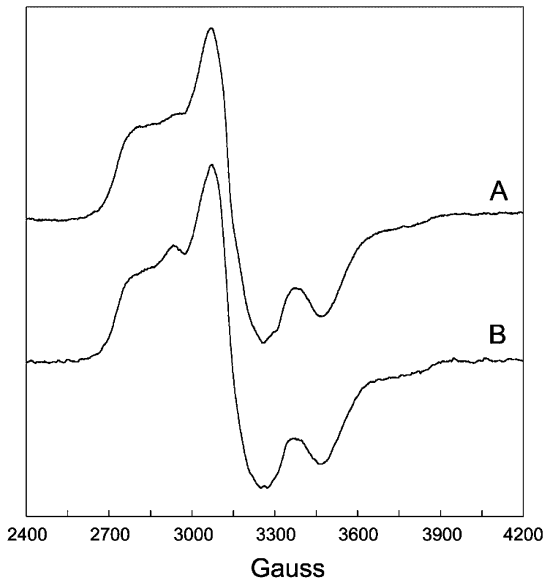

FIGURE 3: EPR spectra of DDH with *an*AdoCbl as the coenzyme in the absence of substrate. The samples were frozen in cold isopentane ~1 min after mixing within an anaerobic chamber: (A) unlabeled coenzyme and (B) [$^{13}C_5$-*ribosyl*]*an*AdoCbl. Experimental conditions: temperature, 4.5 K; modulation amplitude, 12 G; microwave power, 0.2 mW; spectrometer frequency, 9.233 GHz. Both spectra are an average of four 8 min scans.

of active sites hosting the triplet was determined from double integrations to be ~70% in both cases. This value is consistent with the extent of Co−C bond cleavage from similar samples estimated from UV−vis spectroscopy after the same period of incubation (*28*).

To establish the identity of the radical species spin-coupled to cob(II)alamin, EPR spectra were acquired with isotopically

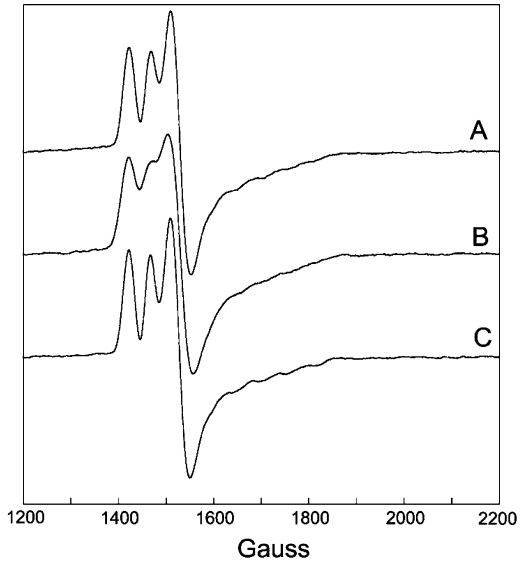

FIGURE 4: EPR spectra of the half-field ($\Delta M_S = 2$) transition for the same samples as described in the legend of Figure 2. Experimental conditions: temperature, 4.5 K; modulation amplitude, 12 G; microwave power, 2 mW; spectrometer frequency, 9.233 GHz. All spectra are an average of four 8 min scans.

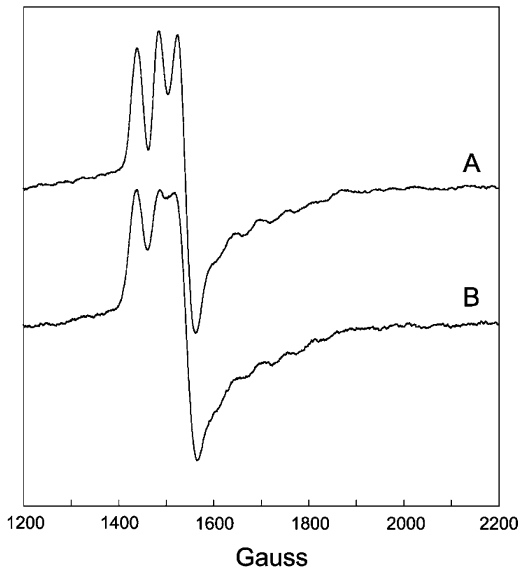

FIGURE 5: EPR spectra of a half-field ($\Delta M_S = 2$) transition for the same samples as described in the legend of Figure 3. Experimental conditions: temperature, 4.5 K; modulation amplitude, 12 G; microwave power, 2 mW; spectrometer frequency, 9.233 GHz. All spectra are an average of four 8 min scans.

labeled coenzyme or substrate. Introduction of ^{13}C ($I = {}^1/_2$) at each position of the anhydroribosyl moiety of *an*AdoCbl ([$^{13}C_5$-*ribosyl*]*an*AdoCbl) leads to inhomogeneous broadening of the EPR signals both in the presence and in the absence of substrate (Figures 2B and 3B, respectively). Only modest ^{13}C-induced broadening effects are observed due to the large overall width of the EPR spectra and the hyperfine splitting contraction characteristic of strongly coupled triplet spin systems. The EPR spectrum obtained with unlabeled *an*AdoCbl and (*R*,*S*)-1,2-[$^2H_6$]propanediol is given in Figure 2C. A subtle line narrowing effect is observed due to incorporation of ^2H into the 5′-position of the coenzyme. Both these effects are more readily visible in the half-field ($\Delta M_S = 2$) transitions where the intrinsic line widths are narrower (Figures 4 and 5). The responses of the line widths to the

Table 1: Parameters Used in the Simulation of the EPR Spectra of DDH with *an*AdoCbl in the Presence and Absence of (*R*,*S*)-1,2-Propanediol

	with (*R*,*S*)-1,2-propanediol	without (*R*,*S*)-1,2-propanediol
Co^{2+} *g* values	$g_x = 2.30$, $g_y = 2.21$, $g_z = 2.00$	$g_x = 2.30$, $g_y = 2.21$, $g_z = 2.00$
radical *g* values	$g_{iso} = 2.00$	$g_{iso} = 2.00$
^{59}Co hyperfine tensor	$A_x = 15$ G, $A_y = 5$ G, $A_z = 113$ G	$A_x = 15$ G, $A_y = 5$ G, $A_z = 113$ G
ZFS parameters	$D = -522$ G, $E = -91$ G	$D = -335$ G, $E = -87$ G
Euler angles	$\zeta = 75°$, $\eta = 10°$, $\xi = 54°$	$\zeta = 71°$, $\eta = -10°$, $\xi = 90°$
exchange coupling	$\|J\| \sim 40-50$ cm^{-1}	$\|J\| \sim 40-50$ cm^{-1}

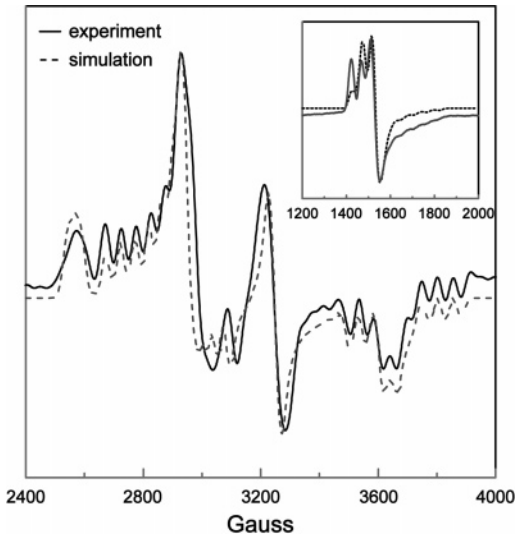

FIGURE 6: Comparison of the simulated and resolution-enhanced experimental EPR spectra of DDH with *an*AdoCbl in the presence of a saturating level of (*R*,*S*)-1,2-propanediol. The ZFS parameters are $D = -522$ G and $E = -91$ G, with Euler angles $\zeta = 75°$, $\eta = 10°$, and $\xi = 54°$. The *g* values for cob(II)alamin and the anhydroadenosyl radical are as follows: $g_x = 2.30$, $g_y = 2.21$, $g_z = 2.00$, and $g_{iso} = 2.00$. The ^{59}Co hyperfine splittings are as follows: $A_x = 15$ G, $A_y = 5$ G, and $A_z = 113$ G. Lorentzian line shapes were used with isotropic line widths of 15 G. The inset compares the simulated and experimental EPR spectrum of the half-field transition, obtained with the same parameter set.

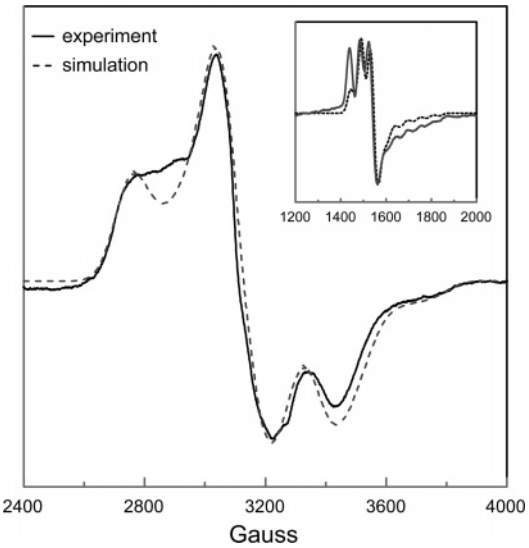

FIGURE 7: Comparison of the simulated and experimental EPR spectrum of DDH with *an*AdoCbl in the absence of (*R*,*S*)-1,2-propanediol. The ZFS parameters are $D = -335$ G and $E = -87$ G, with Euler angles $\zeta = 71°$, $\eta = -10°$, and $\xi = 90°$. The *g* values for cob(II)alamin and the anhydroadenosyl radical are as follows: $g_x = 2.30$, $g_y = 2.21$, $g_z = 2.00$, and $g_{iso} = 2.00$. The ^{59}Co hyperfine splittings are as follows: $A_x = 15$ G, $A_y = 5$ G, and $A_z = 113$ G. Lorentzian line shapes were used with isotropic line widths of 55 G. The inset compares the simulated and experimental EPR spectra of the half-field transition, obtained with the same parameter set.

magnetic isotope substitutions demonstrate that the anhydroadenosyl radical is the other half of the triplet spin system both in the presence and in the absence of substrate.

A weakly allowed half-field ($\Delta M_S = 2$) transition is a spectroscopic signature of strongly coupled triplet spin systems (*35*, *50*). Such transitions are observed in the EPR spectra of DDH with *an*AdoCbl, both in the presence and in the absence of substrate (Figures 4 and 5, respectively). Incubation of DDH with [$^{13}C_5$-*ribosyl*]*an*AdoCbl (Figures 4B and 5B) or unlabeled anAdoCbl and (*R*,*S*)-1,2-[$^2H_6$]-propanediol (Figure 4C) causes line width effects in the half-field transitions analogous to those seen in the $\Delta M_S = 1$ portion of the EPR spectra.

Analysis of the EPR Spectra. Spectral simulations were performed to improve our understanding of the complicated EPR spectra of DDH with *an*AdoCbl as the coenzyme. The parameters used in the simulations are summarized in Table 1. Comparisons of the simulated and resolution-enhanced experimental EPR spectra in the presence and absence of (*R*,*S*)-1,2-propanediol are shown in Figures 6 and 7, respectively. The following *g* values were used in the simulations for the anhydroadenosyl radical: $g_x = 2.30$, $g_y = 2.21$, and $g_z = 2.00$ for Co^{2+} and $g_{iso} = 2.00$ [typical for cob(II)alamin and organic radicals (*23*, *36*, *49*)]. The only hyperfine interaction included in the spectral simulations was that derived from ^{59}Co ($I = 7/2$; $A_x = 15$ G, $A_y = 5$ G, and $A_z = 113$ G); all other hyperfine interactions contribute only to the line widths of the signals in EPR spectra.

The ZFS interactions between cob(II)alamin and the anhydroadenosyl radical are highly rhombic both in the presence ($D = -522$ G, $E = -91$ G, and $E/D = 0.17$) and in the absence ($D = -335$ G, $E = -87$ G, and $E/D = 0.26$) of substrate, indicating that the electron spin densities within the paramagnetic centers are highly delocalized, making the commonly invoked point-dipole approximation invalid (*39*). Euler rotations were required to align the principal axis systems of the ZFS tensors with that of the *g* tensor (or equivalently, the hyperfine splitting tensor) of Co^{2+}, both in the presence ($\zeta = 75°$, $\eta = 10°$, and $\xi = 54°$) and in the absence ($\zeta = 71°$, $\eta = -10°$, and $\xi = 90°$) of substrate. This noncollinearity of tensor axes has a significant influence on the appearance of EPR spectra of strongly coupled triplet systems in that it shifts the apparent *g* values of turning points and transfers hyperfine splittings between turning points (*3*, *39*).

Figure 8 shows the geometries derived from the decomposition of the ZFS tensors obtained from the simulations of the EPR spectra of DDH with *an*AdoCbl in the presence (Figure 8A) and absence (Figure 8B) of (*R*,*S*)-1,2-propanediol. A comparison of these two structures reveals that

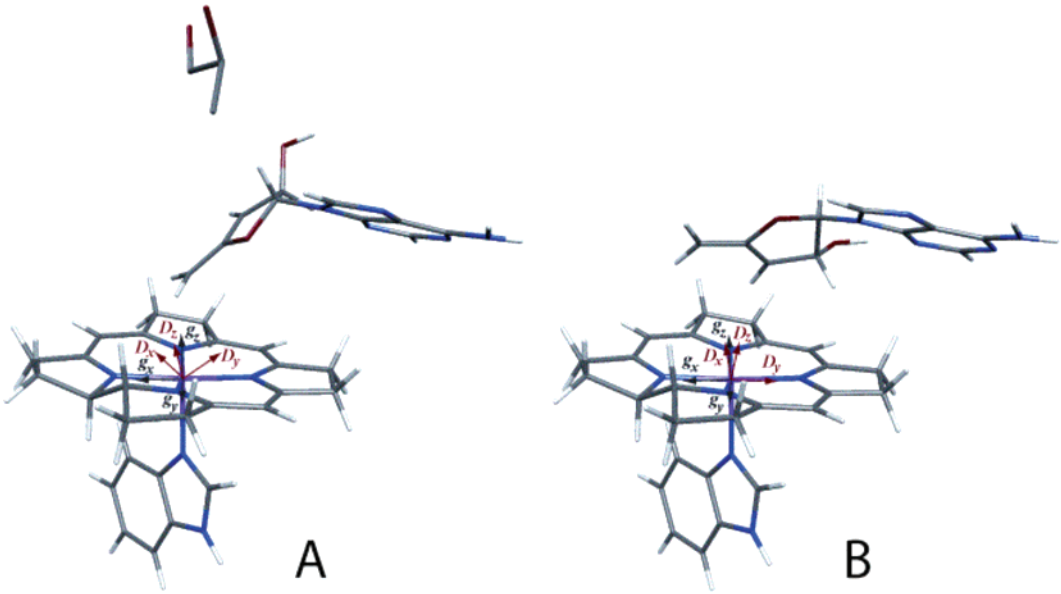

FIGURE 8: Model of cob(II)alamin and the anhydroadenosyl radical in the active site of DDH in the presence (A) and absence (B) of (*R*,*S*)-1,2-propanediol. (A) The distance between C5′ and Co^{2+} is 3.5 Å. The position of the adenine ring is very similar to that observed in the crystal structure of the DDH−adeninylpentylcobalamin complex (rmsd = 0.67 Å) (*44*). (B) The distance between C5′ and Co^{2+} is 4.1 Å. The position of the adenine ring is perturbed slightly (rmsd = 0.53 Å), and the anhydroribosyl moiety rotates ~60° relative to their positions when the substrate is bound. The positions of the *g* and *D* axes are labeled in the corin ring.

upon substrate binding, there is an only slight perturbation in the position of the adenine ring (rmsd = 0.53 Å). The position of the adenine ring of the anhydroadenosyl radical in both the presence and absence of substrate is very similar to that observed in the crystal structure of DDH complexed with adeninylpentylcobalamin (rmsd = 0.67 and 0.84 Å, respectively[3]) (*44*). In addition, when the substrate binds, there is a rotation of the anhydroribosyl moiety by ~60° about the glycosidic bond, which positions the 5′-carbon of the anhydroadenosyl radical closer to Co^{2+} (3.5 Å vs 4.1 Å). This structure is consistent with the larger ZFS observed in the EPR spectrum when substrate is present ($D = -522$ G vs $D = -335$ G). The basis for the greater rhombicity of the ZFS in the absence of substrate ($E/D = 0.26$ vs $E/D = 0.17$) is also evident from a comparison of the two structures. The vector between C5′ and C3′ of the anhydroadenosyl radical (the two atoms with the greatest spin density in the radical) is very nearly perpendicular to the interspin vector with cob(II)alamin in the absence of substrate. In the substrate-bound structure, the C5′−C3′ vector and the interspin vector are closer to being parallel. In the case of electron delocalization about two points, the rhombicity in the ZFS is maximal when these two vectors are orthogonal and vanishes when they are collinear (*39*).

Conclusions. Rotation around the glycosidic bond of the anhydroadenosyl radical would position C5′ of the radical in the proximity of C1 of the substrate. Such a rotation mechanism for propagation of the radical was proposed earlier by Toraya and co-workers on the basis of the crystal structure of the enzyme from *Klebsiella oxytoca* (*44*). The two positions of the anhydroadenosyl radical observed in the presence and absence of substrate in the current study provide direct evidence of this rotation mechanism.

The enzyme may be able to cleave the Co−C5′ bond of AdoCbl without a substrate present, but because of the instability of the 5′-deoxyadenosyl radical, the equilibrium for the bond homolysis reaction would favor the intact coenzyme. This scenario is supported by the results of this study, in which the equilibrium for Co−C5′ bond homolysis of *an*AdoCbl is shifted toward formation of the cleavage products, due to the stability of the resulting allylic radical. Observation of the anhydroadenosyl radical supports the mechanism of DDH, where a transient 5′-deoxyadenosyl radical intermediate functions as the direct abstractor of the hydrogen atom from the substrate. In the case of the *an*AdoCbl, the cofactor-derived radical resides very close to its cob(II)alamin partner in the absence and presence of the substrate.

SUPPORTING INFORMATION AVAILABLE

Numbering of atoms used in the DFT calculation (Figure 1S), DFT-calculated spin densities and/or hyperfine splitting constants (Tables 1S and 2S), and a discussion of the agreement between calculated and experimentally observed hyperfine splitting constants. This material is available free of charge via the Internet at http://pubs.acs.org.

REFERENCES

1. Banerjee, R. (2001) Radical peregrinations catalyzed by coenzyme B_{12}-dependent enzymes, *Biochemistry 40*, 6191−6198.
2. Marsh, E. N. G., and Drennan, C. L. (2001) Adenosylcobalamin-dependent isomerases: New insights into structure and mechanism, *Curr. Opin. Chem. Biol. 5*, 499−505.
3. Reed, G. H. (2004) Radical mechanisms in adenosylcobalamin-dependent enzymes, *Curr. Opin. Chem. Biol. 8*, 477−483.
4. Finke, R. G. (1984) Thermolysis of adenosylcobalamin: A product, kinetic, and Co-C5′ bond dissociation energy study, *Inorg. Chem. 23*, 3041−3043.
5. Padmakumar, R., Padmakumar, R., and Banerjee, R. (1997) Evidence that cobalt-carbon bond homolysis is coupled to hydrogen atom abstraction from substrate in methylmalonyl-CoA mutase, *Biochemistry 36*, 3713−3718.

[3] The orientation of the adenine ring has little effect on the calculated ZFS tensor. However, its position is constrained by the orientation of the glycosidic bond. The dihedral angle used to position the adenine ring was chosen to minimize the rmsd.

6. Marsh, E. N. G., and Ballou, D. P. (1998) Coupling of cobalt-carbon bond homolysis and hydrogen atom abstraction in adenosylcobalamin-dependent glutamate mutase, *Biochemistry 37*, 11864−11872.
7. Bandarian, V., and Reed, G. H. (2000) Isotope effects in the transient phases of the reaction catalyzed by ethanolamine ammonia-lyase: Determination of the number of exchangeable hydrogens in the enzyme-cofactor complex, *Biochemistry 39*, 12069−12075.
8. Toraya, T. (2003) Radical catalysis in coenzyme B_{12}-dependent isomerization (eliminating) reactions, *Chem. Rev. 103*, 2095−2128.
9. Booker, S., Licht, S., Broderick, J., and Stubbe, J. (1994) Coenzyme B_{12}-dependent ribonucleotide reductase: Evidence for the participation of five cysteine residues in ribonucleotide reduction, *Biochemistry 33*, 12676−12685.
10. Chen, D., Abend, A., Stubbe, J., and Frey, P. A. (2003) Epimerization at carbon-5′ of (5′R)-[5′-2H]adenosylcobalamin by ribonucleoside triphosphate reductase: Cysteine 408-independent cleavage of the Co−C5′ bond, *Biochemistry 42*, 4578−4584.
11. Toraya, T. (1999) Diol dehydratase and glycerol dehydratase, in *Chemistry and Biochemistry of B_{12}* (Banerjee, R., Ed.) pp 783−809, Wiley-Interscience, New York.
12. Walling, C., and Johnson, R. A. (1975) Fenton's reagent. Rearrangements during glycol oxidations, *J. Am. Chem. Soc. 97*, 2405−2407.
13. Golding, B. T., and Buckel, W. (1997) Corrin-dependent reactions, in *Comprehensive Biological Catalysis* (Sinnott, M. L., Ed.) pp 239−260, Academic Press, London.
14. Smith, D. M., Golding, B. T., and Radom, L. (2001) Understanding the mechanism of B_{12}-dependent diol dehydratase: A synergistic retro-push-pull proposal, *J. Am. Chem. Soc. 123*, 1664−1675.
15. Kamachi, T., Toraya, T., and Yoshizawa, K. (2004) Catalytic roles of active-site amino acid residues of coenzyme B_{12}-dependent diol dehyratase: Protonation state of histidine and pull effect of glutamate, *J. Am. Chem. Soc. 126*, 16207−16216.
16. Shibata, N., Masuda, J., Tobimatsu, T., Toraya, T., Suto, K., Morimoto, Y., and Yasuoka, N. (1999) A new mode of B_{12} binding and the direct participation of a potassium ion in enzyme catalysis: X-ray structure of diol dehydratase, *Struct. Folding Des.*, 997−1008.
17. Toraya, T., Yoshizawa, K., Eda, M., and Yamabe, T. (1999) Direct participation of potassium ion in the catalysis of coenzyme B_{12}-dependent diol dehydratase, *J. Biochem. 126*, 650−654.
18. Schwartz, P., LoBrutto, R., Reed, G. H., and Frey, P. A. (2003) Suicide Inactivation of Dioldehydrase by 2-Chloroacetaldehyde: Formation of the cis-ethanesemidione radical, and the role of a Monovalent Cation, *Helv. Chim. Acta 86*, 3764−3775.
19. Kawata, M., Kinoshita, K., Takahashi, S., Ogura, K., Komoto, N., Yamanishi, M., Tobimatsu, T., and Toraya, T. (2006) Survey of catalytic residues and essential roles of glutamate-α 170 and aspartate-α 335 in coenzyme B_{12}-dependent diol dehyratase, *J. Biol. Chem. 281*, 18327−18334.
20. Retey, J., Umani-Ronchi, A., Seibl, J., and Arigoni, D. (1966) On the mechanism of the propanediol dehydrase reaction, *Experientia 22*, 502−503.
21. Finlay, T. H., Valinsky, J., Mildvan, A. S., and Abeles, R. H. (1973) Electron spin resonance studies with dioldehydrase: Evidence for radical intermediates in reactions catalyzed by coenzyme B_{12}, *J. Biol. Chem. 248*, 1285−1290.
22. Valinsky, J. E., Abeles, R. H., and Fee, J. A. (1974) Electron spin resonance studies on diol dehydrase III. Rapid kinetic studies on the rate of formation of radicals in the reaction with propanediol, *J. Am. Chem. Soc. 96*, 4709−4710.
23. Pilbrow, J. R. (1982) EPR of B_{12}-dependent enzyme reactions and related systems, in *B_{12}* (Dolphin, D., Ed.) pp 431−463, John Wiley & Sons, Inc., New York.
24. Valinsky, J. E., Abeles, R. H., and Mildvan, A. S. (1974) Electron spin resonance studies of diol dehydrase II. The hyperfine structure of proposed radical intermediates derived from isotopic substitution in 2-chloroacetaldehyde, *J. Biol. Chem. 249*, 2751−2755.
25. Abend, A., Bandarian, V., Reed, G. H., and Frey, P. A. (2000) Identification of cis-ethanesemidione as the organic radical derived from glycolaldehyde in the suicide inactivation of dioldehydrase and of ethanolamine ammonia-lyase, *Biochemistry 39*, 6250−6257.
26. Yamanishi, M., Hirofumi, I., Murakami, Y., and Toraya, T. (2005) Identification of the 1,2-propanediol-1-yl radical as an intermediate in adenosylcobalamin-dependent diol dehydratase reaction, *Biochemistry 44*, 2113−2118.
27. Magnusson, O. T., and Frey, P. A. (2000) Synthesis and characterization of 3′,4′-anhydroadenosylcobalamin: A coenzyme B_{12} analogue with unusual properties, *J. Am. Chem. Soc. 122*, 8807−8813.
28. Magnusson, O. T., and Frey, P. A. (2002) Interactions of diol dehydrase and 3′,4′-anhydroadenosylcobalamin: Suicide inactivation by electron transfer, *Biochemistry 41*, 1695−1702.
29. Magnusson, O. T., Reed, G. H., and Frey, P. A. (2001) Characterization of an allylic analogue of the 5′-deoxyadenosyl radical: An intermediate in the reaction of lysine 2, 3-aminomutase, *Biochemistry 40*, 7773−7782.
30. Poznanskaja, A. A., Tanizawa, K., Soda, K., Toraya, T., and Fukui, S. (1979) Coenzyme B_{12}-dependent diol dehydrase: Purification, subunit heterogeneity, and reversible association, *Arch. Biochem. Biophys. 194*, 379−386.
31. Kauppinen, J. K., Moffaatt, D. J., Mantsch, H. H., and Cameron, D. G. (1981) Fourier self-deconvolution: A method for resolving intrinsically overlapped bands, *Appl. Spectrosc. 35*, 271−276.
32. Latwesen, D. G., Poe, M., Leigh, J. S., and Reed, G. H. (1992) Electron paramagnetic resonance studies of a ras p21-MnIIGDP complex in solution, *Biochemistry 31*, 4946−4950.
33. Goldstein, H., Poole, C. P., Jr., and Safko, J. L. (2002) *Classical Mechanics*, 3rd ed., Addison Wesley, San Francisco.
34. Bandarian, V., and Reed, G. H. (1999) Hydrazine cation radical in the active site of ethanolamine ammonia-lyase: Mechanism-based inactivation by hydroxyethylhydrazine, *Biochemistry 38*, 12394−12402.
35. Wertz, J. E., and Bolton, J. R. (1986) *Electron Spin Resonance*, Chapman and Hall, New York.
36. Gerfen, G. J. (1999) EPR spectroscopy of B_{12}-dependent enzymes, in *Chemistry and Biochemistry of B_{12}* (Banerjee, R., Ed.) pp 165−195, Wiley-Interscience, New York.
37. Bencini, A., and Gatteschi, D. (1990) *EPR of Exchange Coupled Systems*, Springer-Verlag, New York.
38. Mukai, K., and Sogabe, A. (1980) ESR studies of radical pairs of galvinoxyl radical in corresponding phenol matrix, *J. Chem. Phys. 72*, 598−601.
39. Mansoorabadi, S. O., and Reed, G. H. (2003) Effects of electron spin delocalization and non-collinearity of interaction terms in EPR triplet powder patterns, in *Paramagnetic resonance of metallobiomolecules* (Telser, J., Ed.) pp 82−96, American Chemical Society, Washington, DC.
40. Goffe, W. L., Ferrier, G. D., and Rogers, J. (1994) Global optimization of statistical functions with simulated annealing, *J. Econometrics 60*, 65−100.
41. Press, W. H., Flannery, B. P., Teukolsky, S. A., and Vetterling, W. T. (1989) *Numerical Recipes*, Cambridge University Press, New York.
42. Leach, A. R. (2001) *Molecular Modeling Principles and Applications*, 2nd ed., Prentice Hall, London.
43. Frisch, M. J., Trucks, G. W., Schlegel, H. B., Scuseria, G. E., Robb, M. A., Cheeseman, J. R., Zakrzewski, V. G., Montgomery, J. A., Jr., Stratmann, R. E., Burant, J. C., Dapprich, S., Millam, J. M., Daniels, A. D., Kudin, K. N., Strain, M. C., Farkas, O., Tomasi, J., Barone, V., Cossi, M., Cammi, R., Mennucci, B., Pomelli, C., Adamo, C., Clifford, S., Ochterski, J., Petersson, G. A., Ayala, P. Y., Cui, Q., Morokuma, K., Malick, D. K., Rabuck, A. D., Raghavachari, K., Foresman, J. B., Cioslowski, J., Ortiz, J. V., Baboul, A. G., Stefanov, B. B., Liu, G., Liashenko, A., Piskorz, P., Komaromi, I., Gomperts, R., Martin, R. L., Fox, D. J., Keith, T., Al-Laham, M. A., Peng, C. Y., Nanayakkara, A., Gonzalez, C., Challacombe, M., Gill, P. M. W., Johnson, B., Chen, W., Wong, M. W., Andres, J. L., Head-Gordon, M., Replogle, E. S., and Pople, J. A. (1998) *Gaussian 98*, Gaussian, Inc., Pittsburgh, PA.
44. Masuda, J., Shibata, N., Morimoto, Y., Toraya, T., and Yasuoka, N. (2000) How a protein generates a catalytic radical from coenzyme B_{12}: X-ray structure of a diol-dehydratase-adeninylpentylcobalamin complex, *Struct. Folding Des. 8*, 775−788.
45. Gerfen, G. J., Licht, S., Willems, J. P., Hoffman, B. M., and Stubbe, J. (1996) Electron paramagnetic resonance investigations of a kinetically competent intermediate formed in ribonucleotide reduction: Evidence for thiyl radical-cob(II)alamin interaction, *J. Am. Chem. Soc. 118*, 8192−8197.
46. Bothe, H., Darley, D. J., Albracht, S. P., Gerfen, G. J., Golding, B. T., and Buckel, W. (1998) Identification of the 4-glutamyl

radical as an intermediate in the carbon skeleton rearrangement catalyzed by coenzyme B_{12}-dependent glutamate mutase from *Clostridium cochlearium*, *Biochemistry 37*, 4105−4113.

47. Zhao, Y., Abend, A., Kunz, M., Such, P., and Retey, J. (1994) Electron paramagnetic resonance studies of the methylmalonyl-CoA mutase reaction. Evidence for radical intermediates using natural and artificial substrates as well as the competitive inhibitor 3-carboxypropyl-CoA, *Eur. J. Biochem. 225*, 891−896.
48. Padmakumar, R., and Banerjee, R. (1995) Evidence from electron paramagnetic resonance spectroscopy of the participation of radicalintermediates in the reaction catalyzed by methylmalonyl-coenzyme A mutase, *J. Biol. Chem. 270*, 9295−9300.
49. Mansoorabadi, S. O., Padmakumar, R., Fazliddinova, N., Vlasie, M., Banerjee, R., and Reed, G. H. (2005) Characterization of a succinyl-CoA radical-cob(II)alamin spin triplet intermediate in the reaction catalyzed by adenosylcobalamin-dependent methylmalonyl-CoA mutase, *Biochemistry 44*, 3153−3158.
50. Eaton, G. R., and Eaton, S. S. (1989) Resolved electron-electron spin-spin splittings in EPR spectra, *Biol. Magn. Reson. 8*, 650.

BI061586Q